

## LAND COVER MAPPING IN THE BRAZILIAN PAMPA WITH LANDSAT OLI AND TIRS BANDS

MAPEAMENTO DA COBERTURA DE TERRA NO PAMPA BRASILEIRO COM LANDSAT OLI E BANDA TIRS

Patricia Michele Pereira TRINDADE, Daniela Wancura Barbieri PEIXOTO, Tatiana Mora KUPLICH, Claudio Aparecido de ALMEIDA

Instituto Nacional de Pesquisas Espaciais. Avenida Roraima, 1000 - Camobi, Santa Maria - RS. Brasil.  
E-mails: patriciampt.sr@gmail.com; daniwbarbieri@gmail.com; tkuplich@gmail.com; claudio.almeida@inpe.br

Introduction  
Material and methods  
Study area  
Materials  
Methods  
Step 1  
Step 2  
Step 3  
Results and discussion  
Conclusions  
Acknowledgements  
References

**ABSTRACT** - When different time periods are considered, detection of past and present changes in land cover are enabled, also for quantifying and qualifying those changes. Land cover/use maps are the primary tools for the management and conservation of natural and man-made areas. For this, remote sensing bands of the reflected spectrum are usually used, leaving aside the thermal data. The objective of this work was to evaluate the inclusion of the thermal band (b10) of the TIRS (Thermal Infrared Sensor) sensor of Landsat 8 satellite to increase the land cover maps accuracy in the Pampa biome from object-oriented classification. For the development of the research, 11 scenes of the Landsat 8, OLI sensor and TIRS were used. Thus, 14 cells were selected in the Brazilian Pampa, totalling 5% of its area. The following steps were performed: obtaining land surface temperature (LST) data and vegetation indices; data preparation; object-oriented classification; validation with 1354 reference points and analysis of the results. The results showed that the insertion of thermal bands, especially from different dates, increased the discrimination among classes. The classification presented 86% of global accuracy. Therefore, it is recommended to insert thermal data for mapping and environmental monitoring of the Pampa biome.

**Keywords:** Brazilian Pampa. Remote sensing. Surface temperature. Object-oriented classification. Suppression of vegetation.

**RESUMO** - Quando diferentes períodos de tempo são considerados, a detecção de mudanças passadas e presentes na cobertura do solo é habilitada, também para quantificar e qualificar essas mudanças. Os mapas de uso / cobertura do solo são as principais ferramentas para a gestão e conservação de áreas naturais e artificiais. Para isso, normalmente são utilizadas bandas de sensoriamento remoto do espectro refletido, deixando de lado os dados térmicos. O objetivo deste trabalho foi avaliar a inclusão da banda térmica (b10) do sensor TIRS (Thermal Infrared Sensor) do satélite Terrestre 8 para aumentar a precisão dos mapas de cobertura do solo no bioma Pampa a partir da classificação orientada a objetos. Para o desenvolvimento da pesquisa, foram utilizadas 11 cenas do Landsat 8, sensor OLI e TIRS. Assim, foram selecionadas 14 células no Pampa brasileiro, totalizando 5% de sua área. As seguintes etapas foram realizadas: obtenção de dados de temperatura da superfície da terra (LST) e índices de vegetação; preparação de dados; classificação orientada ao objeto; validação com 1354 pontos de referência e análise dos resultados. Os resultados mostraram que a inserção de faixas térmicas, principalmente a partir de datas diferentes, aumentou a discriminação entre as classes. A classificação apresentou 86% de acurácia global. Portanto, recomenda-se inserção de dados térmicos para mapeamento e monitoramento ambiental do bioma Pampa.

**Palavras-chave:** Pampa Brasileiro. Sensoriamento remoto. Temperatura de superfície. Classificação orientada ao objeto. Supressão da vegetação.

### INTRODUCTION

The production of land use and land cover (LULC) maps is one of the most frequent goals of remote sensing (RS) based works. Among the various applications of these maps, we find an indication of the conservation status of ecosystems, as well as sites of sequestration and emission of atmospheric carbon. When different dates of images are considered, quantitative and qualitative detection of changes in LULC is feasible, enabling past and future monitoring of maps' classes. LULC maps are essential tools for the management and conservation of natural and

anthropized areas (Gómez et al., 2016).

Maps of the Brazilian Amazon, presenting forested areas, past and recent deforestation, have been produced since 1988 based on orbital images (mainly from Landsat series), and are the basis for estimating annual deforestation rates (INPE, 2019). These rates are used for the establishment of public policies and, more recently, for government agreements in the area of climate change and greenhouse gases, in the context of REDD+ (Reduction of Emissions from Deforestation and Forest Degradation), required by the United Nations Framework

Convention on Climate Change (UNFCCC) (MMA, 2017). The financial compensation that may come from the mechanisms of REDD+ depends on the standing forest and, recently, consider the other biomes of Brazil as potential areas of conservation for financial compensation.

The Pampa biome, which is covered mainly by grasses and herbaceous vegetation in rangelands, is considered by REDD+ mechanisms, and, as part of that, INPE is conducting its monitoring and mapping, with the first results available on the TerraBrasilis platform. Grasslands are one of the largest coverages on the planet (approximately 32%) and, after the forests, they represent the second-largest carbon reservoir, (Assis et al., 2019) justifying its inclusion in the REDD+ mechanisms.

The Pampa biome occurs in the southern half of Brazilian Rio Grande do Sul state, Uruguai and part of Argentine, and is part of the Temperate grasslands. Its native grasslands (herein called grasslands) are generally explored under continuous and extensive grazing, in some locations in mixed crop systems with rice, soybean, and wheat. In recent years part of Pampa have been converted to other uses, such as agriculture and monocultures of exotic trees (pine and eucalyptus). The conversion rate of grasslands to agricultural areas has been of the order of 1000 km<sup>2</sup> per year (Cordeiro & Hasenack, 2009) demonstrating the urgent need to map their remnants to guide management and conservation policies. By 2018, the Pampa biome had approximately 46% of its native vegetation converted to other uses (INPE, 2019).

The challenges of mapping grasslands with remote sensing (RS) images are immense. The wide variety of Pampa grassland physiognomies

(Hasenack et al., 2010; Moreira et al., 2019), includes grasslands with prostrate grasses, with clumps (cespitosus), wetlands and with different types of management, dependent on soils, climate, and phenological stages. The spectral behavior of these complex physiognomies can hinder their discrimination in RS images. Moreover, confusion can occur when discriminating between grasslands and croplands.

Visual/manual discrimination of degraded or converted grasslands for other uses in RS images is a widely used method, and, if combined with field data, ensures high accuracy in the generated maps (Kuplich et al., 2016). However, for frequent monitoring and operational surveillance, the automatic classification of RS images is used with relative success for mapping grasslands in various regions of the world (Assis et al., 2019). Important requirements for accurate classification of grassland vegetation are the use of different seasons multispectral optical images, to cover grasses phenological stages and rangelands management types. Combined with this, land surface temperature (LST) images can be used to complement this process, improving the efficiency of LULC classification (Ehsani & Quiel, 2010; Eisavi et al., 2015; Sun & Schulz, 2015; Zhao et al., 2019). Different researches (Mangafić et al., 2018; Käfer et al., 2020) also highlighted the use of thermal bands for the study of grasslands.

The objective of this work was to evaluate the inclusion of the thermal band (b10) of TIRS (Thermal Infrared Sensor) sensor of Landsat 8 satellite as to increase the discrimination between Pampa vegetation classes and the accuracy of the LULC maps generated.

## MATERIAL AND METHODS

### Study area

For the development of this research, fourteen 25 km x 25 km cells were selected as study areas in the Brazilian Pampa (Figure 1), corresponding to approximately 5% of the biome.

The Pampa is the only Brazilian biome covering only one state, Rio Grande do Sul, occupying 63% of its territory. It was recognized as a biome only in 2004, but it is part of one of the most important temperate grasslands in the world, with a predominance of rangelands, wetlands, riparian forest and woodlands (MMA, 2019).

### Materials

For the development of this research, 11 Landsat 8 images (OLI and TIRS sensors) were

used for different dates (2017 and 2018). The images were downloaded from the United States Geological Survey (USGS) site with bands 2 (blue 0.45 - 0.51  $\mu\text{m}$ ), 3 (green 0.53 - 0.59  $\mu\text{m}$ ), 4 (red 0.64 - 0.67  $\mu\text{m}$ ), 5 (near infrared 0.85 - 0.88  $\mu\text{m}$ ) 6 (medium infrared 1.57 - 1.65  $\mu\text{m}$ ) and 7 (medium infrared 2.11 - 2.29  $\mu\text{m}$ ) in surface reflectance (SR) of the OLI sensor and band 10 (thermal infrared 10.60 - 11.19  $\mu\text{m}$ ) of the TIRS sensor in brightness temperature (BT). The processing was done with Ecognition and QGIS 2.14 softwares.

### Methods

Figure 2 presents a flowchart with the methodological steps of this research, which are explained next.

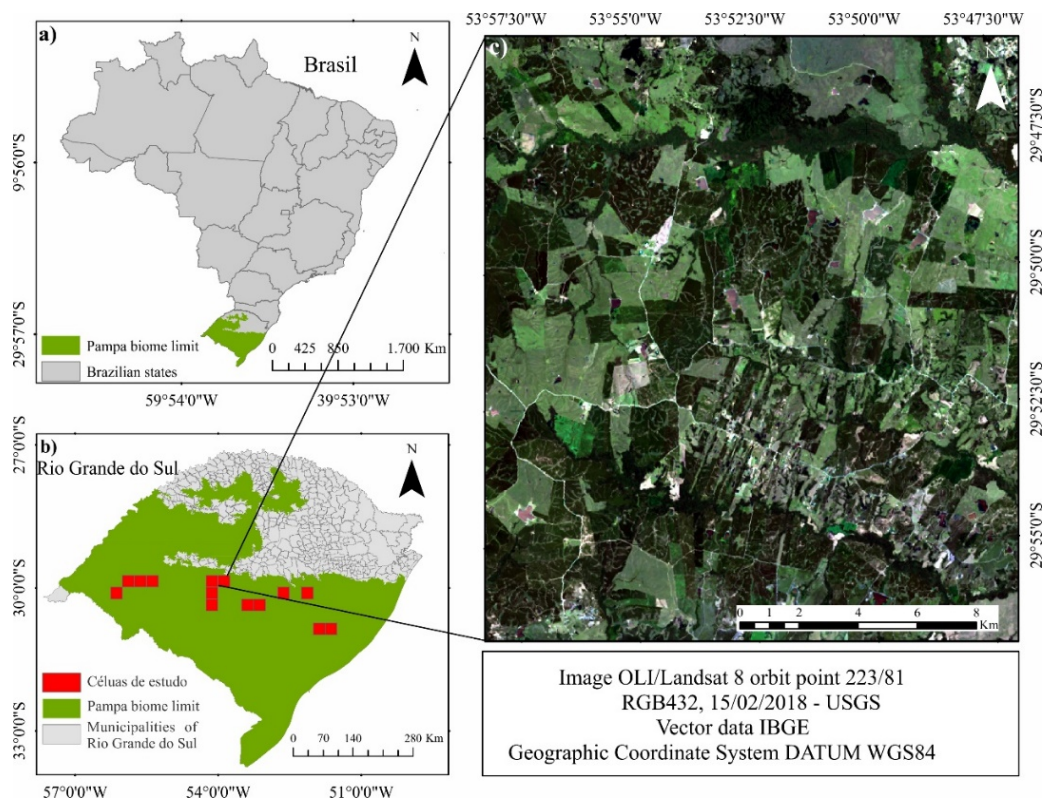


**Figure 1** - Study area location: a) Location of Brazilian Pampa; b) Location of study cells in the Pampa Biome; c) Initial cell of the classifications.

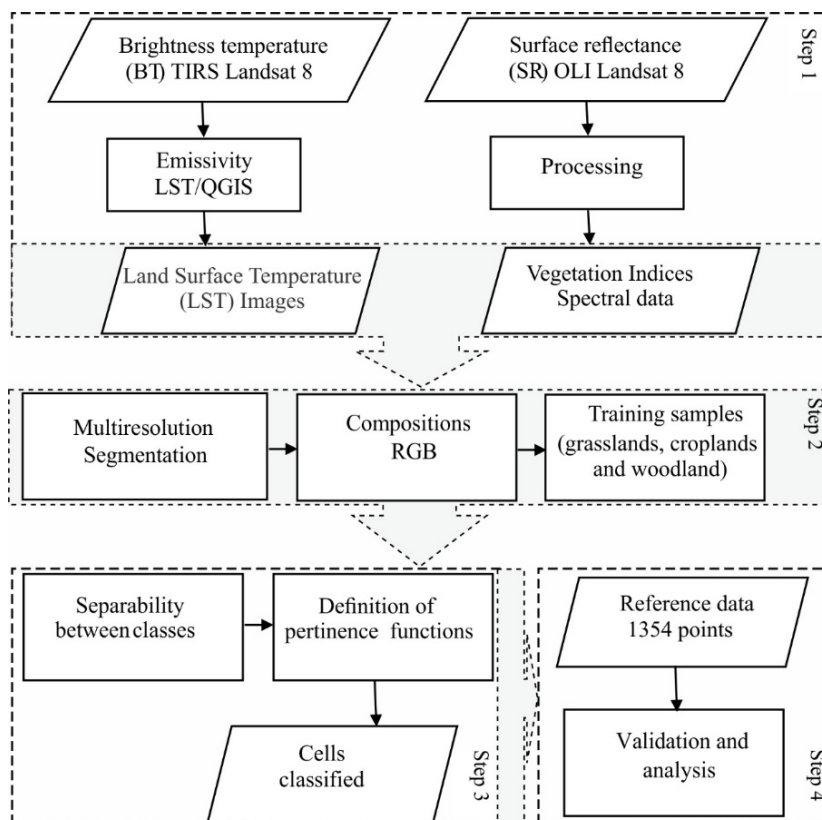


**Figure 2** - Flowchart of methodological procedures.

### Step 1

Several studies (Van de Griend & Owen, 1993; Sobrino et al., 2008; Ndossi & Avdan, 2016; Gerace & Montarano, 2017; Dong et al., 2020; Käfer et al., 2020) applied or developed prototypes to recover LST considering variables such as São Paulo, UNESP, *Geociências*, v. 40, n. 4, p. 1115 - 1124, 2021

emissivity, meteorological and atmospheric data, underlining the advantages of each method. In this work, the LST estimates were performed in the QGIS software based on the methodology presented by (Ndossi & Avdan, 2016).

For estimating LST, it was considered the

correction of emissivity only, according to equation 1.

The emissivity image was obtained from the relationship with the Normalized Difference Vegetation Index (NDVI) (Equation 1 and Table 1), according to the methodology used in other studies (Van de Griend & Owen, 1993; Guo et al., 2020; Valor & Caselles, 1996; Sobrino et al., 2004; Zhang & Xiao, 2007).

$$LST = \frac{BT}{1 + \left(\frac{\lambda BT}{\alpha}\right) \cdot \ln \varepsilon} \quad (1)$$

where ST is the land surface temperature; BT is the at-sensor brightness Temperature (K);  $\lambda$  is the wavelength of the emitted radiance;  $\alpha$  is the  $hc/K = 1.438 \times 10^{-2}$  mK;  $\varepsilon$  and is the spectral emissivity.

$$NDVI = \frac{b5 - b4}{b5 + b4} \quad (2)$$

where b5 is the near infrared band; and b4 is red band.

**Table 1** - NDVI and Emissivity relationship.

NDVI	Emissivity
NDVI < -0.185	0.995
-0.185 ≤ NDVI < 0.157	0.985
0.157 ≤ NDVI ≤ 0.727	1.009 + 0.047 x ln(NDVI)
NDVI > 0.727	0.990

Source: Adapted from Ndossi & Avdan (2016).

### Step 2

The image classification was performed in the Ecognition software, so first, the segmentation of the images was done using the Multiresolution Segmentation algorithm, considering different values of scalar factor, shape, and compactness. The scale factors were tested for values of 50, 100, 150, and 200, considering compactness of 0.8 and form 0.3.

After segmentation, homogeneous regions were selected, representing objects that could be classified, avoiding the salt and pepper effect found in pixel-by-pixel classifications (Blaschke et al., 2000; Blaschke, 2010).

Using the different colored band compositions, including SR and LST bands, training samples were collected for grasslands, croplands, and forest

classes (herein referred as woodlands, as they included reduced tree patches as well). For the areas covered by water, a mask of "non-vegetation" was created, so they were not considered in the classifications.

### Step 3

The Feature Space Optimization tool (from Ecognition) allowed to verify the separability between classes using combinations of different surface SR and BT bands.

The three classes established in step 2 and the different spectral bands considered, generated different band combinations with distinct values of separation between the classes. The bands chosen were the ones that presented the highest values in relation to the separation of classes, that is, the bands that presented less confusion between the classes.

For the study area classification, the object-oriented method was used, which considers pertinence functions or fuzzy logic.

The equations were established from the combination of spectral bands (band mathematics) that demonstrated better separability between classes. When using fuzzy functions, each object can be associated with different degrees of pertinence, these ranging from 1 (belongs) to 0 (does not belong). The greatest degree of pertinence define the class to which the object belongs (Pinho et al., 2005). Different works, Tang et al. (2016), highlighted that object-oriented classification generally produced maps with greater accuracy than pixel-by-pixel ratings.

### Step 4

For validating the classification, random reference points were distributed regularly on the test cells, comprising 1354 points with a distance of 1.5 Km. Thus, each point was interpreted considering high-resolution images of the Google Earth tool, Landsat 8 images with different band compositions and seasons, and 2016/2018 deforestation data available on the Terra Brasilis Platform (MMA, 2019; Almeida et al., 2020). The reference points were compared with each classified cell, generating a confusion matrix that allowed to calculate the classification global accuracy and producer and user accuracies.

## RESULTS AND DISCUSSION

Tests with different segmentations identified that scalar 100 was adequate for representing the classes visualized in the images. It was possible to individualise targets such as small dams and

large grasslands.

For the study area, following the seasons at the South of Brazil, the crops presented high vegetative vigor in January and February and, in

the months of July to September, these areas began to be covered by winter pastures. From November onwards, the soil is generally bare as the preparation for crops sowing starts (MAPA, 2015). In the work carried out in areas of the Argentinian Pampa, (Guerschman et al., 2003) found that the combination of images from November / December with January / February

highlighted the croplands. Due to this agricultural calendar, the visible bands (green and blue) and the thermal band were associated to the RGB channels respectively, considering different dates (that is, January or February for the visible bands and November or December for the thermal band). Thus, it was possible to differentiate the classes easily (Figure 3).

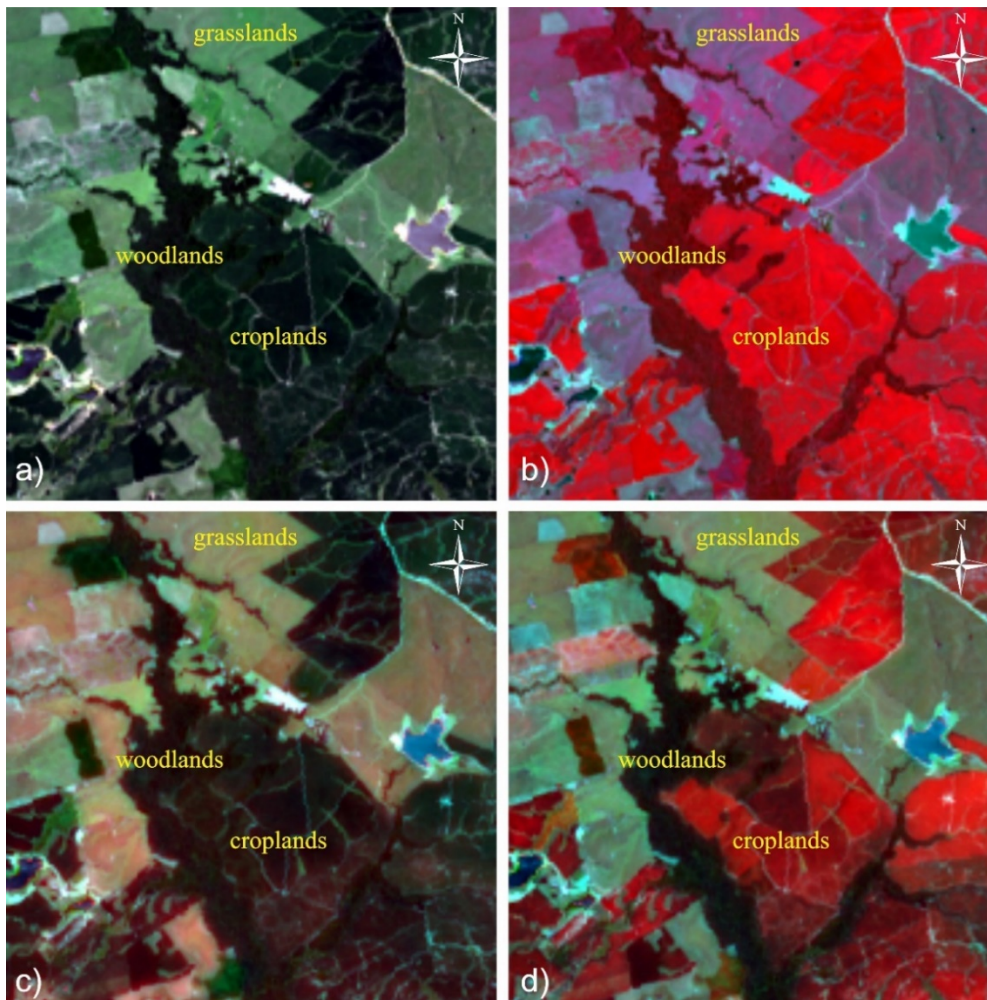


**Figure 3** - RGB Compositions: a) RGB 4 3 2 with February bands; b) RGB 5 4 3 with February bands; c) RGB Band10 3 2 with February bands; d) RGB 10 3 2 with the band 10 of December and bands 3 and 2 of February. (\* The goal was to find the best composition to differentiate areas of grasslands, croplands and woodlands).

As an example, it was found that the cropland and woodland classes were not easily differentiated in the February (F) composition (Figure 3a). In composition 2 (Figure 3b), generally used for vegetation studies, the differentiation between classes has already improved. Associating the February temperature band with the R channel (Figure 3c) accentuated the grassland class. Contrarily, when adding the December thermal band (D) to the R channel, there was a higher differentiation between the classes. In figure 3d, it is possible to verify the difference between croplands (red color), woodlands (dark green) and grasslands (light green), which were not well differentiated in the previous compositions. The

same findings occurred in January/December and January/November compositions, although the combination of the February reflectance band and December thermal band presented higher differentiation for vegetation.

The good performance of the compositions was confirmed after separability results obtained with Ecognition Feature Space Optimization tool, where it was possible to verify the best band combinations to differentiate grasslands, woodlands and croplands. When only the bands of the reflected spectrum (SR) were used (all dates), the separability between classes presented an approximate value of 2.67 (Figure 4). When adding the thermal bands, separation between classes increased

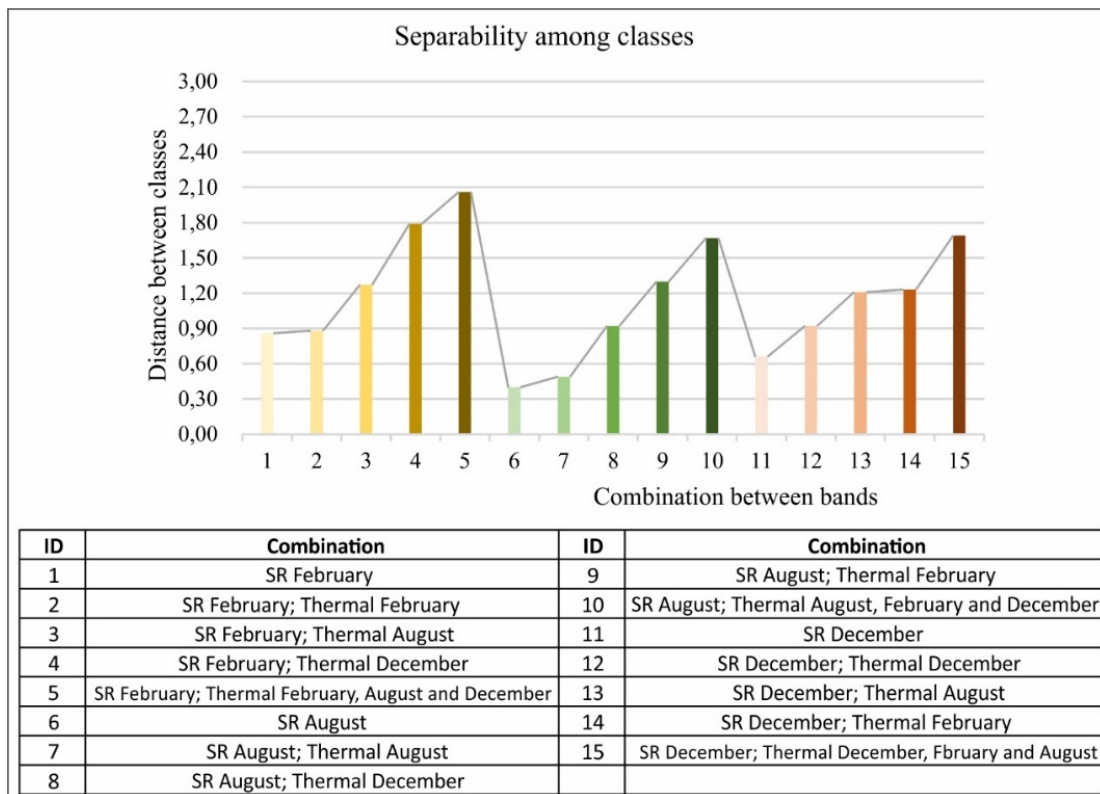


**Figure 4** - Separability among classes according to bands combination.

to 2.98. However, when considering only the thermal bands, the separability decreased to 0.87, that is, the thermal data added quality to the classification, but it cannot be considered as the main element. It is also noteworthy that the separability between classes presented the best result with the combination of images from different times of the year.

For example, when considering only August SR bands, the separability approached 0.39, being increased to 1.30 with the inclusion of the February thermal band. In February SR bands, the separability increased from 0.86 to 1.79 when the thermal band of the December was added. Only the December SR bands presented separability of 0.65, with the thermal band the value was approximately 1.23. When considering the NDVI for the separability of the classes, the values were lower than those obtained in the combinations of the multispectral bands with the thermal bands.

From the classes' separability results using different band combinations (findings described

above), descriptors were defined. Descriptors are mathematical relationships that enhance attributes of objects in the scene (Pinho et al., 2005). An example of a descriptor is the Simple Ratio vegetation index, defined from the ratio of the near-infrared band with the red band. In this sense, different mathematical combinations were tested until the descriptors that best discriminated the classes were chosen.

It can be said that the borders of croplands are stable, however, the type of crop changes frequently (Blaschke, et al., 2000). Therefore, in times of high vegetative vigor, the temperature of vegetation is lower than temperature of bare soil (after harvesting and when preparing for the next crop). Thus, to classify the croplands, the descriptor 1 (Table 2) was used, which considered the difference between the December and February thermal bands. The grasslands were identified using descriptor 2 (Table 2) from February bands 2, 3, and 7 and the December thermal band. The descriptor 3 (Table 2), was used to classify the woodlands.

**Table 2** - Descriptors used for classifying croplands, grasslands and woodlands.

Descriptor	DN range	Class
$D1 = b10(\text{dec}) - b10(\text{feb})$	> 1.7	Cropland
$D2 = b2 + b3 + b7(\text{dec})/b10(\text{dec})$	61 a 100	Grassland
$D3 = b2(\text{feb}) + b7(\text{dec})/b10(\text{dec})$	22 a 44	Woodland

Fourteen (14) study cells (Figure 5) were classified using the information provided by the descriptors (table 2) in the following order: (1st) using the descriptor for classifying woodlands, (2nd) grasslands, and (3rd) crops. Results showed grasslands covering most of the studied cells (38.7%), followed by croplands (36.7%) and woodlands in 11.81% of the total classified area.

With the standardization of descriptors values

for all cells, it was not possible to classify 100% of the study area, so at least 8% of the areas were not classified. With this finding, it can be inferred that the unclassified areas represent more heterogeneous coverage and that they do not present a common pattern to the three types of classes considered in the present study. An alternative for the classification of these areas would be to test new intervals for descriptors, which can be developed in future studies.

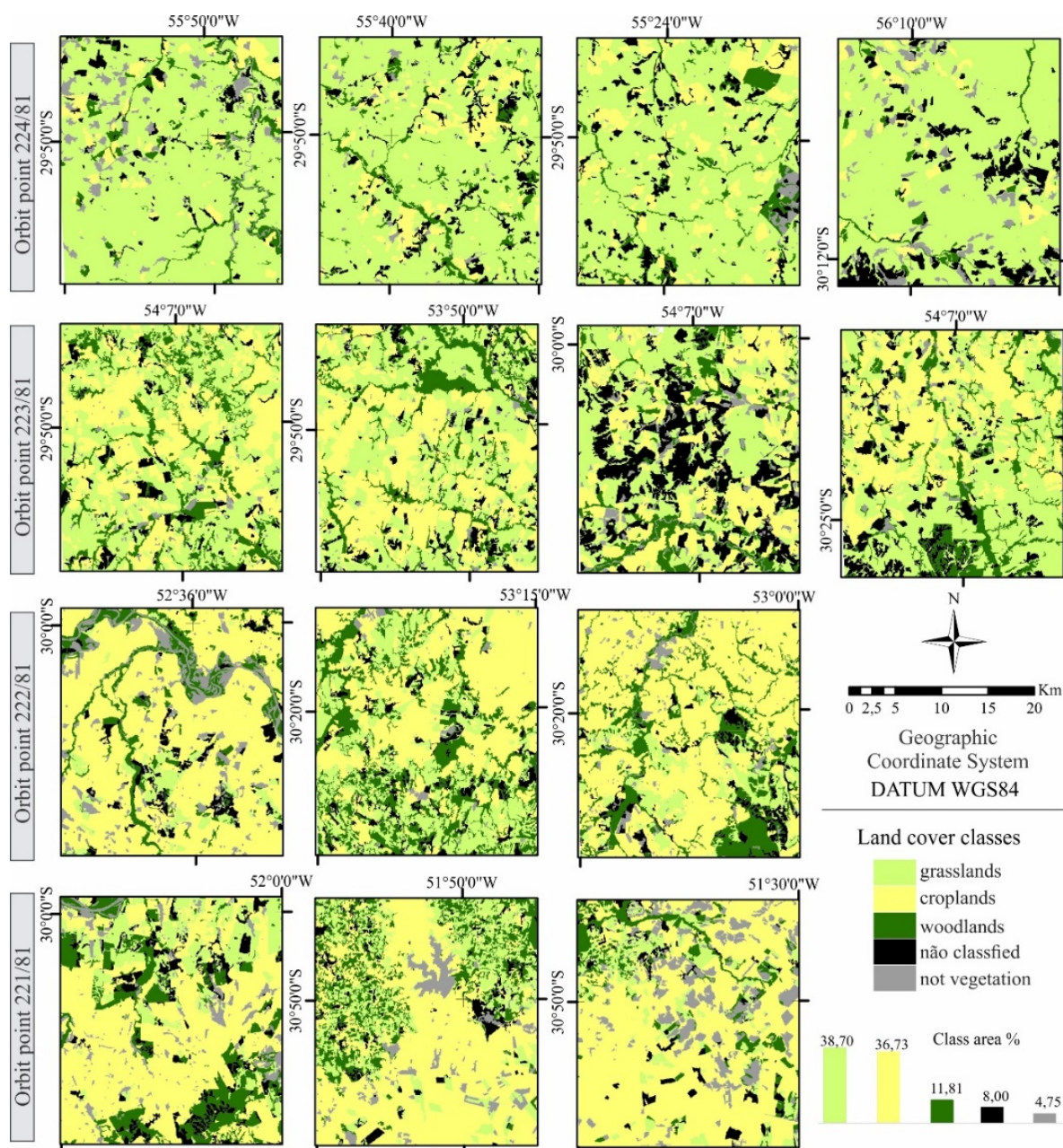


Figure 5 - Fourteen cells classified according to descriptors in table 2.

A confusion matrix (Table 3) with user, producer and global accuracies values was generated. In general, it was found that the classification presented an excellent performance, with 86% of correct answers (Table 4). In this sense, it was found that the croplands class presented the greatest omission error (18%) in

relation to the other classes, with user accuracy of 91.7% and producer of 81.6%, followed by the woodland class with 83.2% and 86.3% accuracy of the user and producer, respectively. It is noteworthy that the grasslands presented greater confusion with the croplands class, with lower omission error (7%) than the remaining classes.

**Table 3** - Confusion matrix for croplands, grasslands and woodlands.

Classification		Reference			
		croplands	grasslands	woodlands	Total
croplands		535	35	13	583
grasslands		92	469	13	574
woodlands		28	5	164	197
Total		655	509	190	1354

**Table 4** - Evaluation of the classification.

User %	Comission error %	Producer %	Omission error %
91,77	8.23	81.68	18.32
81,71	18.29	92.14	7.86
83,25	16.75	86.32	13.68
Global accuracy		0.86	

The results showed that the thermal band can contribute to the classification of land cover in Pampa, and in 92% of the cells classified, with a global accuracy greater than 85%. The inclusion of the thermal band can improve the accuracy of a classification by 5 to 6%<sup>11</sup>. It is also noteworthy that the object-oriented classification combined with the inclusion of the thermal band, especially considering the combination of images from different dates, can help to automate the classification of vegetated covers.

On object-oriented classification methodology, previous studies (Zhang, & Xiao, 2007; Dornik et al., 2018; Blaschke, 2010) an increase in overall accuracy when compared to traditional ratings. For instance, from the reference survey on different types of classification, Blaschke (2010), pointed out that the object-oriented classifications presented accuracy greater than 90%. When comparing different classifications in western Romania, Dornik et al. (2018) found a

higher overall accuracy of 10% in object-oriented classification in relation to pixel-by-pixel classification.

In relation to the thermal band, different works (Rodríguez Galiano et al., 2012; Eisavi et al., 2015; Zhao et al., 2019) highlighted the increased accuracy in land use and cover mapping after including this band in the analysis. For example, by combining the multispectral bands with the TM/Landsat 5 thermal band, Rodríguez-Galiano et al. (2012) found a 10% increase in accuracy in the classification of land cover in the Province of Granada located in southern Spain. By using the thermal bands of the TIRS/Landsat 8 sensor, Eisavi et al. (2015) found a 4% to 8% increase in land use classification accuracy in the city of Naghadeh, western Azerbaijan.

Figure 6b shows that the areas with suppressed vegetation had higher temperatures when compared to the 2016 image (Figure 6a), as a result they were identified as deforestation in 2018 (Figure 6c).

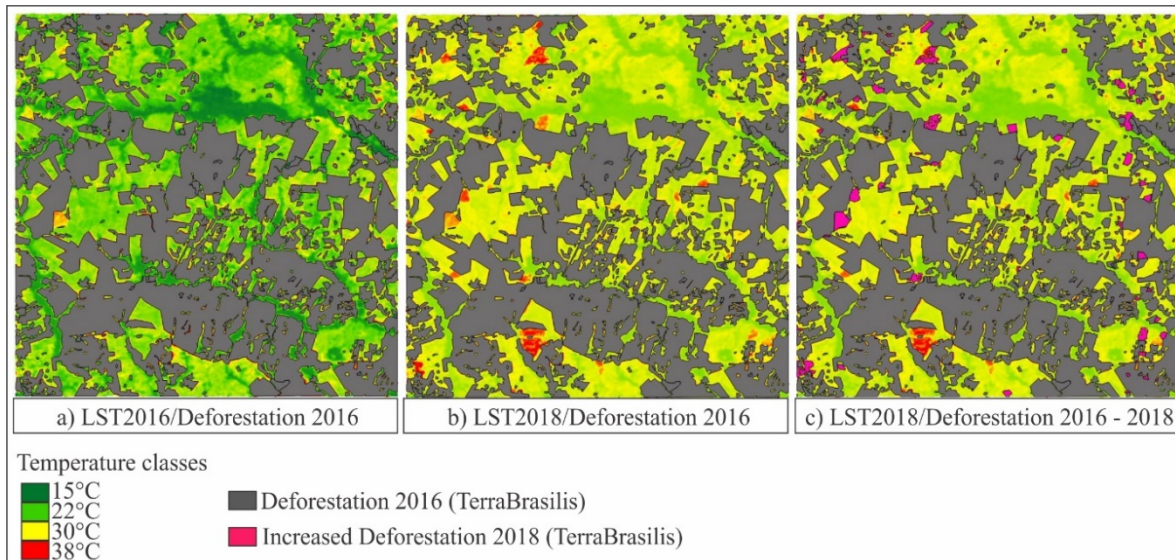


**Figure 6** - Comparison among TIRS / Landsat 8 temperature images and TerraBrasilis deforestation mask 2016 – 2018: a) LST of 11/24/2016 and deforestation mask 2016; b) LST of 12/16/2018 and 2016 deforestation mask; c) LST of 12/16/2018 and deforestation mask 2016 and 2018.

Thus, it was verified the potential of the thermal band to discriminate areas where grassland vegetation was removed (converted to other use/cover) in the Brazilian pampa, both in automatic classification and visual analysis,

when comparing the temperature images with the TerraBrasilis deforestation mask (resulting in 85% overall accuracy). This fact demonstrates the applicability of thermal bands in environmental monitoring projects in Brazil and worldwide.

## CONCLUSIONS

The study demonstrated increased discrimination of vegetated classes in the Brazilian Pampa using the thermal data as surface temperature. Also, the use of thermal bands enabled the automatic classification of the selected areas in the Pampa biome with global accuracy of 86%. It is also noteworthy that the use of images from different times of the year, both surface reflectance and temperature, was decisive to identify and discriminate the objects generated from images segmentation. Allied to this, fuzzy pertinence functions demonstrated efficacy in object-oriented classification, as they allowed the attribution of values for each class from the choice of the best descriptors.

In addition to the mapping of each previously

defined class, the use of thermal bands allowed identifying areas of deforestation. According to this, it was found that deforestation areas can be detected by integrating existing deforestation masks with the segmented LST images (when considering the minimum and maximum values of the histograms of each image). The best timing for succeeding with this identification at the study area (South of Brazil) was when the soil was prepared for sowing, around November and December.

Therefore, it is recommended the use of thermal data for monitoring and mapping vegetation in the Pampa biome. For future work it is suggested to test the methods in different areas of the Pampa biome and whenever, as to account for diverse environmental characteristics.

## ACKNOWLEDGEMENTS

PMPT and DWBP are funded by the Brazilian National Council for Scientific and Technological Development (CNPq) with grants from Project "Monitoramento dos Biomas Brasileiros por Satélite: Construção de Novas Capacidades (444418/2018-0)". We thank Flora Martins from FUNCATE (Foundation for Science, Technology and Space Applications) for suggestions and data.

## REFERENCES

- ASSIS, L.F.F.G.; FERREIRA, K.R.; VINHAS, L.; MAURANO, L.; ALMEIDA, C.; CARVALHO, A.; CAMARGO, C. TerraBrasilis: A Spatial Data Analytics Infrastructure for Large-Scale Thematic Mapping". *ISPRS International Journal of Geo-Information*, v. 8, n. 11, p. 513, 2019.
- ALMEIDA, C.A.; VALERIANO, D.M.; MAURANO, L.; VINHAS, L.; FONSECA, L.M.G.; SILVA, D.; SANTOS, C.P.F.; MARTINS, F. S. R. V.; LARA, F.C.B.; MAIA, J.S.; PROFETA, E.R.; SANTOS, L.O.; SANTOS, F.C.O.; RIBEIRO, V. Deforestation monitoring in different Brazilian Biomes: challenges and lessons. In: *ISPRS ANNALS OF THE PHOTOGRAMMETRY, REMOTE SENSING AND SPATIAL INFORMATION SCIENCES*, Santiago, Chile, 2020, *Actas...* Santiago, 2020, v. IV-3/W2.
- BLASCHKE, T.; LANG, S.; LORUP, E.; STROBL, J.; ZEIL, P. **Object-oriented image processing in an integrated GIS/remote sensing environment and perspectives for environmental applications**. Kremers, & K. Greve (Eds.), *Umweltinformation für Planung, Politik und Öffentlichkeit / Environmental Information for Planning, Politics and the Public*, v. 2, p. 555 - 570. Metropolis, 2000.
- BLASCHKE, T. Object based image analysis for remote sensing". *ISPRS JOURNAL OF PHOTOGRAMMETRY AND REMOTE SENSING*, v. 65, n. 1, p. 2-16, 2010. Doi:10.1016/j.isprsjprs.2009.06.004
- CORDEIRO, J.L.P. & HASENACK, H. Cobertura vegetal atual do Rio Grande do Sul. In: *Campos Sulinos conservação e uso sustentável da biodiversidade*, ed. by PILLAR, V. D.; MÜLLER, S. C.; CASTILHOS, Z. M. S.; JACQUES, A. V. A. Brasília: Ministério do Meio Ambiente Chap. 23, 2009.
- DONG, P.; GAO, L.; ZHAN, W.; LIU, Z.; LI, J.; LAI, J.; LI, H.; HUANG, F.; TAMANG, S.K.; ZHAO, L. Global comparison of diverse scaling factors and regression models for downscaling Landsat-8 thermal data. *Journal of Photogrammetry and Remote Sensing*, v. 169, p. 44 - 56, 2020.
- DORNIK, A.; DRĂGUȚ, L.; URDEA, P. Classification of Soil Types Using Geographic Object-Based Image Analysis and Random Forests". *Pedosphere*, v. 28, n. 6, p. 913-925, 2018.
- EHSANI, A.H. & QUIEL, F. Efficiency of Landsat ETM+ Thermal Band for Land Cover Classification of the Biosphere Reserve "Eastern Carpathians" (Central Europe) Using SMAP and ML Algorithms". *International Journal of Environmental Research*, v. 4, n. 4, p. 741-750, 2010.
- EISAVI, V.; HOMAYOUNI, S.; YAZDI, A.M.; ALIMOHAMMADI, A. Land cover mapping based on random forest classification of multitemporal spectral and thermal images. *Environmental Monitoring and Assessment*, v. 187, n. 5, p. 1-14, 2015.
- GERACE, A. & MONTARANO, M. Derivation and validation of the stray light correction algorithm for the thermal infrared sensor onboard Landsat 8. *Remote Sensing of Environment*, v. 191, p. 246-257, 2017.
- GÓMEZ, C.; WHITE, J.C.; WULDER, M.A. Optical remotely sensed time series data for land cover classification: A review. *ISPRS Journal of Photogrammetry and Remote Sensing*, v. 116, p. 55-72, 2016.
- GUERSCHMAN, J.P.; PARUELO, J.M.; DI BELLA, C.; GIALLORENZI, M.C. Land cover classification in the Argentine Pampas using multi-temporal Landsat TM data. *Int.*

- J. Remote Sensing**, v. 24, p. 3381–3402, 2003.
- GUO, J.; REN, H.; ZHENG, Y.; LU, S.; DONG, J. Evaluation of Land Surface Temperature Retrieval from Landsat 8/TIRS Images before and after Stray Light Correction Using the SURFRAD Dataset. **Remote Sensing**, v. 12, p. 1 – 21, 2020.
- HASENACK, H.; WEBER, E.; BOLDRINI, I.; TREVISAN, R. **Mapa de sistemas ecológicos da ecorregião das Savanas Uruguaias em escala 1:500.000**. Porto Alegre: UFRGS/Centro de Ecologia, 2010. PROJETO IB/CECOL/TNC, PRODUTO 4, 2010.
- INPE (Instituto Nacional de Pesquisas Espaciais). Coordenação geral de Observação da Terra. **Programa de Monitoramento da Amazônia e demais biomas. Desmatamento – Bioma Pampa**. 2019. Accessed 10 January 2020. <http://terrabrasilis.dpi.inpe.br/downloads/>. Acesso em: 05 fev. 2020.
- KÄFER, P. S., ROCHA, N. S., DIAZ, L. R., KAISER, E. A., COSTA, S. T. L., HALLAL, G., VEECK, G., ROBERTI, D., & ROLIM, S. B. A. Seasonal assessment of surface temperature with normalized vegetation index and surface albedo over pampa biome. In H. J. Hernandez Palma, C. A. Cardenas Mansilla, A. Frery, & R. Q. Feitosa (Eds.), *International Archives of the Photogrammetry, Remote Sensing and Spatial Information Sciences - ISPRS Archives*. (International Archives of the Photogrammetry, Remote Sensing and Spatial Information Sciences - ISPRS Archives). International Society for Photogrammetry and Remote Sensing. v.2, p. 471-476, 2020. Doi: <https://doi.org/10.5194/isprs-archives-XLII-3-W12-2020-471-2020>
- KUPLICH, T.M.; BARBIERI, D.W.; MOREIRA, A.; QUADROS, F.L.F.; TRENTIN, A.B.; CORAZZA, R.; DEPRÁ, B. **Algumas aplicações de sensoriamento remoto em estudos de vegetação campestre no RS**". São José dos Campos: INPE (2016). Accessed 15 December 2019. <http://urlib.net/rep/8JMKD3MGP3W34P/3LQEG78>
- MAPA (Ministério da Agricultura, Pecuária e Abastecimento). **Calendário Agrícola**, 2015. Accessed 15 December 2019. [https://www.laborsolo.com.br/arquivos/formularios/calendario\\_plantio\\_20150407.pdf](https://www.laborsolo.com.br/arquivos/formularios/calendario_plantio_20150407.pdf).
- MANGAFIĆ, A.; MESNER, N; TRIGLAV ČEKADA, M. Grassland Recognition with the Usage of Thermal Weights. In: *FREE AND OPEN SOURCE SOFTWARE FOR GEOSPATIAL (FOSS4G) Conference Proceedings.....*, v. 18, article 3, .2018. DOI: <https://doi.org/10.7275/em16-x776>
- MMA (Ministério do Meio Ambiente). **Pampa**. Folder Pampa. (2019) Accessed 15 Abril 2020. <https://www.mma.gov.br/biomas/pampa>
- MMA (Ministério do Meio Ambiente), **Estratégia Do Programa de Monitoramento Ambiental Dos Biomas Brasileiros** (2017). Edited by Ministério do Meio Ambiente MMA. 2a. Brasília. Accessed 5 November 2019. [http://www.mma.gov.br/images/arquivos/gestao\\_territorial/pmabb/Estrategia\\_programa\\_monitoramento\\_ambiental\\_PMABB.pdf](http://www.mma.gov.br/images/arquivos/gestao_territorial/pmabb/Estrategia_programa_monitoramento_ambiental_PMABB.pdf).
- MOREIRA, A.; BREMM, C.; FONTANA, D.C.; KUPLICH, T.M. Seasonal dynamics of vegetation indices as a criterion for grouping grassland typologies. **Scientia Agricola**, v. 76, n. 1, p. 24–32, 2019.
- NDOSSI, M.I. & AVDAN, U. Application of open source coding technologies in the production of Land Surface Temperature (LST) maps from Landsat: A PyQGIS plugin". **Remote Sensing**, v. 8, n. 5, p. 1 – 31, 2016.
- PINHO C.; FEITOSA, F.; KUX, H. "Classificação automática de cobertura do solo urbano em imagem IKONOS: Comparação entre a abordagem pixel-a-pixel e orientada a objetos". In: SIMPÓSIO BRASILEIRO DE SENSORIAMENTO REMOTO, XII, Goiânia, 2005. **Anais...Goiânia: Sociedade Brasileira de Geologia**, 2005, p. 4217– 4224.
- RODRÍGUEZ-GALIANO, V.F.; GHIMIRE, B.; PARDO-IGÚZQUIZA, E.; CHICA-OLMO, M.; CONGALTON, R.G. Incorporating the downscaled Landsat TM thermal band in land-cover classification using random forest. **Photogrammetric Engineering and Remote Sensing**, v. 78, n. 2, p. 129–137, 2012.
- SOBRINO, J.A.; JIMÉNEZ-MUÑOZ, J.C.; PAOLINI, L. Land Surface Emissivity Retrieval from Different VNIR and TIR Sensors. *IEEE Trans. Geosci. Remote Sens.*, v. 46, n. 2, p. 316–327, 2008.
- SOBRINO, J.A.; JIMÉNEZ-MUÑOZ, J.C.; PAOLINI, L. Land surface temperature retrieval from LANDSAT TM 5. **Remote Sensing of Environment**, v. 90, n. 4), p. 434–440 (2004).
- SUN L. & SCHULZ K. The Improvement of Land Cover Classification by Thermal Remote Sensing. **Remote Sensing**, v. 7, p. 8368-8390, 2015.
- TANG, Y.; JING, L.; LI, H.; ATKINSON, P.M. A multiple-point spatially weighted k-NN method for object-based classification. **International Journal of Applied Earth Observation and Geoinformation**, v. 52, p. 263–274, 2016.
- VALOR, E. & CASELLES, V. "Mapping land surface emissivity from NDVI: Application to European, African, and South American areas". **Remote Sensing of Environment**, v. 57, n. 3, p. 167–184, 1996.
- VAN DE GRIEND, A.A. & OWEN, M. On the relationship between thermal emissivity and the normalized difference vegetation index for natural surfaces. **International Journal of Remote Sensing**, v. 14, n. 6, p. 1119–1131, 1993.
- ZHANG, K.; AN, J.; XIAO, Y. Object-oriented urban dynamic monitoring - A case study of Haidian District of Beijing. **Chinese Geographical Science**, v. 17, n. 3, p. 236–242, 2007.
- ZHAO, J., YU, L., XU, Y., REN, H., HUANG, X., & GONG, P. Exploring the addition of Landsat 8 thermal band in land-cover mapping. **International Journal of Remote Sensing**, v. 40, n. 12, p. 4544–4559, 2019.

*Submetido em 12 de maio de 2021  
Aceito para publicação em 5 de novembro de 2021*